RSC Advances

ROYAL SOCIETY OF CHEMISTRY

www.rsc.org/advances

Tuning chemistry of graphene oxides by sonochemical approach: Application on adsorption properties

Yubing Sun[1,2,3*], Shubin Yang[2], Congcong Ding[2], Zhongxiu Jin,[2] Wencai Cheng[4,51]

1. *Institute of Plasma Physics, Chinese Academy of Science, P.O. Box 1126, Hefei, 230031, P.R. China*
2. *School of Environment and Chemical Engineering, North China Electric Power University, Beijing 102206, P.R. China.*
3. *School for Radiological and Interdisciplinary Sciences, Soochow University, 215123, Suzhou, P.R. China*
4. *Collaborative Innovation Center of Radiation Medicine of Jiangsu Higher Education Institutions, P.R. China*
5. *Faculty of Engineering, King Abdulaziz University, Jeddah 21589, Saudi Arabia*

ABSTRACT: The change in chemical properties of graphene oxides (GOs) can be tuned by the sonochemical approach. The layers of GOs were significantly decreased by the sonochemical approach from the high resolution transmission electron microscopy and atomic force microscopy analysis. The abundant hydroxyl groups and carboxyl groups were introduced with increasing ultrasonic time by the analysis of Raman, FTIR, UV-vis absorbance spectroscopy and XPS techniques. The adsorption of U(VI) on GOs significantly increased at pH 1.0 - 6.0, whereas decreased adsorption was observed at pH > 8.0. The adsorption capacities of GOs increased with increasing ultrasonic time. According to EXAFS analysis, the interaction mechanism between

* Corresponding author. Tel: +86 551 65592788; fax: +86 551 65591310. E-mail: sunyb@ipp.ac.cn (Y. B. Sun)

radionuclides and GOs was inner-sphere surface complexation. Such an efficient approach to control the chemical properties of GOs further promotes its applications in environmental cleanup.

1. Introduction

Owing to the excellent water-solubility, large specific surface area, enriched oxygenated functional groups, it is demonstrated that graphene oxides (GOs) presents high efficient adsorption capacities for heavy metals and radionuclides [1-4]. Zhao et al. [1] demonstrated that the few-layered GOs presented high adsorption performance for heavy metals. Sun et al. [2] also found that the maximum adsorption capacity of few-layered GOs at pH 4.5 and T = 298 K was 175 mg/g for Eu(III), which was much higher than those of other today's materials. It is demonstrated that such high adsorption performance is attributed to a variety of hydrophilic oxygenated functional groups such as massive hydroxyl and epoxy groups at the basal plane and the small amounts of carboxyl and carbonyl groups at the sheet edges [5-9]. To the best of the author's knowledge, few studies on the effect of these oxygenated functional groups on the adsorption properties of GOs by sonochemical approach were observed [10-14].

Herein, we presented an efficient approach to control the amount of oxygenated functional groups of GOs by using sonochemical approach at different time intervals. The sonochemical approach has been extensively employed to functionalize the various nanostructured materials [15-17]. The objectives of this study were (1) to characterize the change in surface properties and nanostructures of GOs at different

ultrasonic time via high resolution transmission electron microscopy (HRTEM), atomic force microscopy (AFM), Raman spectroscopy, Fourier transformed infrared spectroscopy (FTIR), UV-vis absorbance spectroscopy and X-ray photoelectron spectroscopy (XPS); (2) to investigate the adsorption properties of GOs under different ultrasonic time; (3) to determine adsorption mechanism between radionuclides and GOs with a variety of oxygenated functional groups by extended X-ray absorption fine structure (EXAFS) spectroscopy. The highlight of this paper is that the adsorption capacity of GOs significantly increase with increasing ultrasound time at low frequency conditions.

2. Experimental

2.1 Materials

Expandable graphite (< 20 μm) was provided from Qingdao Tianhe Graphite Co., Ltd (Shandong, China). The expandable graphite was used as starting material instead of flake graphite to ensure more uniform oxidization [12, 18]. Sulfuric acid (~ 98%), sodium nitrate, potassium permanganate, sodium borohydride and hydrogen peroxide (H_2O_2, 37 %) were purchased from Sinopharm Chemical Reagent Co., Ltd. Milli-Q water was used in this study. U(VI) stock solution (0.1 mol/L) was prepared from uranium nitrate ($UO_2(NO_3)_2 \cdot 6H_2O$, 99.99 % purity, Sigma-Aldrich) after dissolution and dilution with Milli-Q water.

2.2 Synthesis procedures

The GOs were synthesized by the chemical oxidation of expandable graphite in terms of modified Hummers' method [19]. Briefly, the expandable graphite (300 mesh, ~

2.0 g) and $NaNO_3$ (co-solvent, 1.5 g) was added into concentrated H_2SO_4 (150 mL) under vigorous stirring and ice-water bath conditions, then $KMnO_4$ (9.0 g) was slowly added over about 2 h. The suspension was continually stirred for 5 days at room temperature. Then the suspension was heated to 98 °C, and 280 mL 5 wt% H_2SO_4 solution was added over about 2 h under vigorous stirring conditions. The residual MnO_4^- ions were removed by adding H_2O_2 solution (12 mL, 30 wt %) at 60 ºC. After reactions, the mixture was centrifuged and washed with 10 % HCl solution to remove residual metal ions. The precipitate was then washed with distilled water and centrifuged repeatedly until pH neutral. The few layers of GOs were obtained in the supernatant with an ultrasonic treatment (PS-1008HT dual-frequency ultrasonic cleaner, Hefei climbed Ultrasonic Technology Co., Ltd.) at 40 kHz for 30 min and followed by centrifugation at 13000 rpm for 60 min and then dialysis it over several weeks [20]. The aforementioned GO suspensions were sonicated 0, 8, 16 and 24 h (noted as GO0, GO1, GO2 and GO3, respectively) by using PS-1008HT dual-frequency ultrasonic cleaner operating at a low frequency of 20 KHz. All ultrasonic experiments were conducted at ultrasonic power between 100 and 110 mW/mL measured by calorimetry. The oxygenated functional groups in GOs facilitate the exfoliation into monolayers under the sonochemical approach. The advantage of ultrasound is that it prevents aggregation of GOs by the introduction of OH carboxyl and epoxy groups in between the layers of GOs, which may not be achieved by the conventional chemical methods. Details on the synthesis of GOs were well-documented in our published reports [1, 4].

2.3 Characterization

The morphologies and nanostructures of GO0, GO1, GO2 and GO3 were investigated by AFM (Digital instrumental Nanoscope III) and HRTEM (JEOL 2010 FEG microscope). The samples for HRTEM and AFM analysis were prepared by dispensing a small amount of suspension on 200 mesh copper grids and mica substrate, respectively. A variety of oxygenated functional groups of GO0, GO1, GO2 and GO3 were analyzed using XPS with a monochromatic Mg XZ-ray radiation (thermo ESCALAB 250 electron spectrometer) at 10 kV and 5 mA under 10^{-8} Pa residual pressure. The peak energies of XPS spectra were corrected with C 1s peak at 284.6 eV as a reference. The deconvolution of C 1s and O 1s lines were performed using XPSPEAK41 program after substraction of the background (Shirley baseline correction). The FTIR spectra of the samples were recorded in pressed KBr pellets (Aldrich, 99%, analytical reagent) by using a PerkinElmer Spectrum 100 system spectrometer at room temperature. The Raman spectra were conducted using a LabRam HR Raman spectrometer with excitation at 514.5 nm for 10 s by Ar^{+} laser to avoid overheating of the GOs. The absorbance of the GO0, GO1, GO2 and GO3 in aqueous solution (~ 5 mg/L) was characterized using UV-vis spectroscopy (Varian, Cary 5000). Uranium L_{III}-edge EXAFS of samples were conducted at Shanghai Synchrotron Radiation Facility. The spectra of samples were collected in fluorescence mode with Silicon (111) double-crystal monochromator. The analysis and fitting of EXAFS data were performed using Athena and Artemis interfaces to IFFEFIT 7.0 software [21, 22].

2.4 Batch adsorption experiments

The batch adsorptions of U(VI) onto GO0, GO1, GO2 and GO3 (0.25 g/L) were conducted under pH 4.0 and T = 293 K within the U(VI) concentration ranging from 1 to 100 mg/L. Briefly, the bulk suspensions of GO0, GO1, GO2 and GO3 with $NaClO_4$ were pre-equilibrated for 24 hr, then U(VI) stock solutions were spiked into the bulk suspension gradually to avoid the formation of schoepite precipitate. Subsequently, the suspensions were shaken for 48 h to ensure that the adsorption reaction could achieve adsorption equilibrium (preliminary experiments demonstrated that 6 h was adequate for the suspension to obtain adsorption equilibrium). To eliminate the effect of U(VI) adsorption on polycarbonate tube walls, the adsorption of U(VI) without adsorbents was carried out under the same experimental conditions. The solid and liquid phases were separated by centrifugation at 9000 rpm for 30 min. The concentration of U(VI) was analyzed by kinetic phosphorescence analyzer (KPA-11, Richland, USA). All experimental data were the average of triplicate determinations and the error bars (5 %) were provided.

3. Results and Discussion

3.1 Characterization

The characterization of GO0, GO1, GO2 and GO3 were conducted via HRTEM, AFM, Raman spectroscopy, FT-IR, UV-vis absorbance spectroscopy and XPS. The morphology and nanostructure of GO0 and GO3 were visualized in terms of HRTEM (Figure 1A and B). It can be clearly seen that the lattice lines decreased from several tens of nanometers for GO0 (~10 nm, Figure 1A) to around 1.0 nm for GO3 (~ 1.0 nm,

Figure 1B), which could be correspond to multilayer and monolayer of GOs respectively, which was consistent with the results of Stankovich et al. [23]. The slightly higher thickness of monolayer GOs (~ 1.2 nm) could be due to the presence of oxygenated functional groups [24]. Results from HRTEM images revealed that the lateral dimensions of GOs decreased by the sonochemical approach.

Figure 1C and D showed the AFM images of GO0 and GO3, respectively. As shown in Figure 1C, the thickness of GO0 was ca. 1-2 nm, whereas approximately 1.0 nm was observed for GO3 (Figure 1D). The results of AFM analysis indicated that the bi- and mono-layer GO nanosheets can be obtained by the sonochemical approach. The significant differences in the morphology of GO0, GO1, GO2 and GO3 were further demonstrated in terms of SEM images in Figure S1 in Supporting Information (SI). The BET specific surface area of GO0, GO1, GO2 and GO3 was measured to 124.7, 126.1, 132.5, and 144.8 m^2/g, respectively. The larger specific surface area of GO3 could be due to the formation of smaller size at elevated ultrasonic time conditions, which increases their adsorption capacity.

It is well-known that Raman spectroscopy is the nondestructive and most direct technique to characterize the structure of carbon-based materials. As shown in Figure 2A, the Raman spectra of GO0, GO1, GO2 and GO3 displayed a D-band (disordered sp^3-hybridized carbon) at ~ 1360 cm^{-1} and a broad G-band (graphitic sp^2-hybridized carbon) at ~ 1590 cm^{-1}. The significant blue shift of G band (e.g., 1594 and 1604 cm^{-1} for GO0 and GO1, respectively) was observed, indicating the layers of GOs were decreased by the sonochemical approach [25, 26]. It was demonstrated that the D band

154 (sp^3-hybridized carbons) was resulted from the structural defection created by the
155 attachment of hydroxyl and epoxy groups on the carbon basal plane [27]. Therefore,
156 the integrated intensity ratio of the D- and G-bands (I_D/I_G) indicated the oxidation
157 degree of sp^2 ring clusters in a network of sp^3 and sp^2 bonded carbon [28]. The slight
158 enhance of I_D/I_G of GO0 (0.920) and GO3 (0.926) suggested that the abundant
159 structural defection of GOs was observed due to the presence of massive oxygenated
160 functional groups. The 2D band at approximately 2700 cm^{-1} was the inset in Figure3A.
161 The significant change of 2D band of GO3 (approximately 2760 cm^{-1}) was due to the
162 decrease of thickness of AB stacked flakes [31]. The change in oxygenated functional
163 groups can be demonstrated by FTIR spectra. As shown in Figure 2B, GO0, GO1,
164 GO2 and GO3 presented the various oxygenated functional groups such as hydroxyl
165 (at 3450 - 3150 cm^{-1}), carboxyl (at ~ 1725 cm^{-1}), C=C (at ~1635 cm^{-1}), ether or epoxy
166 group (at 1250-1050 cm^{-1}) [29, 30]. The sharp peaks centered at 1400 cm^{-1} was
167 corresponded to the C-O vibration mode [32]. The relative intensities at ~ 1725, 1635,
168 1050 cm^{-1} increased with increasing ultrasonic time, indicating that more carboxyl
169 and epoxy groups were generated by the sonochemical approach. It should be noted
170 that the relative intensities of GO3 at 3150 cm^{-1} was decreased, whereas the relative
171 intensity of GO3 at 1725 cm^{-1} was significantly increased. It was quite evident from
172 FTIR analysis that the amount of hydroxyl groups was decreased, whereas the amount
173 of carboxyl and epoxy groups was increased with increasing ultrasonic time.
174 According to the UV-vis absorbance spectra (Figure 2C), the relative intensities of
175 absorbance spectra of GOs were decreased by the sonochemical approach. The

maximum peak at 224 nm (inset in Figure 2C) corresponded to $\pi \rightarrow \pi^*$ transitions of aromatic C-C bonds [33]. Figure 2D showed the deconvolution of C 1s XPS spectra of GO0, GO1, GO2 and GO3. The spectra presented five different components, including sp^2-hybridized carbons in aromatic rings (C-C, 284.6 eV), hydroxyl (C-OH, 285.0 eV), epoxy (C-O-C, 286.5 eV), carbonyl (-C=O, 287.0 eV) and carboxyl groups (COOH, 288.5 eV), which can be comparable to previous reports [34-36]. The deconvolution of O 1s spectra (Figure S2 in SI) also exhibited four peaks around 531.08, 532.03, 533.43 and 534.7 eV, which can be assigned to oxygen doubly bonded to aromatic carbon (C=O), oxygen singly bonded to aliphatic carbon (C-O-C), oxygen singly bonded to aromatic carbon (C-OH) and chemisorbed/intercalated adsorbed water molecules (adsorbed H_2O), respectively. It should be noted that the relative peak intensities of C-C groups significantly decreased with increasing ultrasonic time, whereas the enhanced relative peak intensities of C-O and O-C=O groups were observed. The results form XPS analysis indicated that the abundant hydroxyl groups and carboxyl groups were introduced by the sonochemical approach.

The change in the oxygenated functional groups of GOs under sonochemical approach was further demonstrated by XRD patterns in Figure S3 in SI. According to XRD patterns, the diffraction peak of GOs at $2\theta \sim 12.31^\circ$ shifted to lower angle with increasing ultrasonic time, indicating that the intersheet distance for GOs film slightly increased with increasing of ultrasonic time. The slightly increase in distance was due to the presence of massive oxygenated functional groups in GOs [37]. It was observed that the full width at half maximum of GOs at $2\theta = 12.31^\circ$ significantly increased with

198 increasing ultrasonic times, which indicating that the smaller size of GOs was
199 observed [38]. On the basis of various characterization results, it was quite clear that
200 the fewer layers and the smaller size of GOs was obtained at elevated ultrasonic time,
201 and the abundant hydroxyl groups and carboxyl groups were introduced under the
202 sonochemical approach.

203 *3.2 pH effect*

204 Figure 3A showed the effect of pH on U(VI) on GO0, GO1, GO2 and GO3 in the
205 presence of 0.01 mol/L $NaClO_4$ solution. One can see that the adsorption of U(VI)
206 significantly increased with increasing pH from 1.0 to 6.0, then high-level adsorption
207 was observed at pH 6.0 -7.0. The decreased adsorption of U(VI) on GO0, GO1, GO2
208 and GO3 at pH > 8.0 was due to the electrostatic repulsion between negatively
209 charged GOs and negatively charged U(VI) species at high basic conditions, which
210 was consistent with previous studies [22, 39, 40]. It was demonstrated the GOs
211 synthesized by Hummers method was negatively charged through the wide range of
212 pH from 2.0 to 9.0 [41, 42]. The distribution of U(VI) species in aqueous solutions
213 was calculated in our previous studies [4, 22]. One can see that the main U(VI)
214 species was UO_2^{2+} at pH < 4.0, whereas a variety of positively charged U(VI) species
215 (i.e., $UO_2(OH)^+$, $(UO_2)_3(OH)_5^+$ and $(UO_2)_4(OH)_7^+$ species) were observed at pH 5.0 –
216 7.0. Therefore, the increased adsorption of U(VI) on GOs at pH 2.0 – 7.0 was likely
217 due to the electrostatic attraction between negatively charged GOs and positively
218 charged U(VI) species.

219 *3.3 Adsorption isotherms*

To investigate the application of GOs in the environmental cleanup, we conducted the adsorption behaviors of U(VI) on GOs by batch techniques. As shown in Figure 3B, the adsorption of U(VI) on GOs significantly increased with increasing initial concentration. The adsorption behaviors of U(VI) on GO0, GO1, GO2 and GO3 can be satisfactorily fitted by Langmuir model (R^2 > 0.997, Table S1 in SI). As summarized in Table S1, the maximum adsorption capacities of GO0, GO1, GO2 and GO3 calculated from Langmuir model at pH 4.0 and T = 293 K were approximate 102.0, 126.6, 137.0 and 151.5 mg/g, respectively, which were significantly higher than those of other today's adsorbents reported currently. The increased adsorption capacity of GO3 could be attributed to its high specific surface area (144.8 m^2/g) as compared to GO1 (124.7 m^2/g). However, the normalized maximum adsorption capacities (Qs = Qe/S_{BET}) of GO0, GO1, GO2 and GO3 were calculated to be 0.818, 0.999, 1.034 and 1.046 mg/m^2, respectively. Therefore the increased Qs values were not only attributed to their specific surface area but also their chemical properties. Sonochemical approach normally leaded to hydroxylation of GOs due to the generation of OH radicals by acoustic cavitation. The hydroxyl and carboxyl groups of GOs were responsible for the enhanced adsorption of U(VI) by following Eqn. (1) and (2), respectively:

$$S\text{-}OH + UO_2^{2+} = S\text{-}OUO_2^{+} + H^{+} \quad (1)$$

$$S\text{-}COOH + UO_2^{2+} = S\text{-}COOUO_2^{+} + H^{+} \quad (2)$$

where S-OH and S-COOH referred to the hydroxyl and carboxyl groups of GOs. The abundant hydroxyl groups and carboxyl groups were introduced, which increased the

adsorption of U(VI) with increasing ultrasonic time. Therefore, the enhanced adsorption capacity of GOs for radionuclides could be attributed to their large specific surface area and massive oxygenated functional groups with increasing ultrasonic time, which was consistent with the characteristic results.

3.4 Interaction mechanism

The interaction mechanism between GOs and U(VI) was elucidated by uranium L_{III}-edge EXAFS spectra (Figure 4A). As shown in Figure 4A, the EXAFS spectra of GO0, GO1, GO2 and GO3 displayed the similar distinct cyclic evolution, whereas a poor signal-to-noise ratio of GO0, GO1, GO2 and GO3 was observed at $\kappa > 8$ Å^{-1}. Figure 4B showed the Fourier transforms (FT, uncorrected phase shift) of EXAFS spectra for U(VI)-reacted GOs. As shown in Figure 4B, the EXAFS spectra of GO0, GO1, GO2 and GO3 displayed the similar features. The corresponding fitted results were also shown in Figure 4B (dash lines) and Table 1. The bond distance (R + ΔR) in the FT feature at ~ 1.4 and 1.9 Å can be satisfactorily fitted by two axial oxygen (U-Oax at ~1.80 Å) and 4-5 equatorial oxygen (U-Oeq, at ~ 2.42 Å in Table 1), respectively. We attempted to fit equatorial U-Oeq shell into two shells (U-Oeq1 and U-Oeq2) caused the convergence of two shells at the same bond distance. For samples of GO0, GO1, GO2 and GO3, the FT peak at ~ 2.5 Å (R +ΔR) can be fitted by U-C shell very well [43], revealing the formation of inner-sphere surface complexes between GOs and U(VI). The fitting results indicated that the adsorption mechanism between U(VI) and GOs was inner-sphere surface complexation.

4. Conclusions

Based on the characterization results, the abundant hydroxyl groups and carboxyl groups were introduced by the sonochemical approach. The results indicated that the increase of adsorption performance of GOs was observed by the sonochemical approach. The adsorption mechanism between U(VI) and GOs was determined to be inner-sphere surface complexation by the analysis of EXAFS spectra. This paper gives the insights into the further development of GOs in environmental cleanup by the selective decoration of oxygenated functional groups.

Acknowledgments

Financial support from Scientific Research Grant of Hefei Science Center of CAS (2015SRG-HSC009; 2015SRG-HSC006), National Natural Science Foundation of China (21207135, 21225730 and 91126020), Anhui Provincial Natural Science Foundation (1408085MB28) and Hefei Center for Physical Science and Technology (2012FXZY005) are acknowledged.

Electronic Supplement Materials: Additional characterization data of SEM, XPS and XRD, the fitting of adsorption data by Langmuir and Freundlich models.

REFERENCES

1 G. X. Zhao, J. X. Li, X. M. Ren, C. L. Chen and X. K. Wang, *Environ. Sci. Technol.,* 2011, **45**, 10454-10462.

2 Y. B. Sun, Q. Wang, C. L. Chen and X. K. Wang, *Environ. Sci. Technol.*, 2012, **46**, 6020-6027.

3 A. Y. Romanchuk, A. S. Slesarev, S. N. Kalmykov, D. V. Kosynkin and J. M. Tour,

Phys. Chem. Chem. Phys., 2013, **12**, 2321-2327.

4 Y. B. Sun, D. D. Shao, C. L. Chen, S. B. Yang and X. K. Wang, *Environ. Sci. Technol.*, 2013, **47**, 9904-9910.

5 A. Lerf, H. He, M. Forster and J. Klinowshi, *J. Phys. Chem. B,* 1998, **102**, 4477-4482.

6 I. Jung, M. Vaupel, M. Pelton, R. Piner, D. A. Dikin, S. Stankovich, J. An and R. S. Ruoff, *J. Phys. Chem. C*, 2008, **112**, 8499-8506.

7 G. Eda and M. Chhowalla, *Adv. Mater.* 2010, **22**, 2392-2415.

8 O. C. Compton and S. T. Nquyen, *Small*, 2010, **6**, 711-723.

9 D. Chen, H. B. Feng and J. H. Li, *Chem. Rev.* 2012, **112**, 6027-6053.

10 C. S. Lim, A. Ambrosi and M. Pumera, *Phys. Chem. Chem. Phys.,* 2014, **16**, 12178-12182.

11 K. Krishnamoorthy, G. S. Kim and S. J. Kim, *Ultrason. Sonochem*., 2013, **20**, 644-649.

12 S. Anandan, A. Manivel and M. Ashokkumar, *Fuel Cells,* 2012, **6**, 956-962.

13 K. Vinodgopal, B. Neppolian, I. V. Lightcap, F. Grieser, M. Ashokkumar and P. V. karnat, *J. Phys. Chem. Lett.,* 2010, **1**, 1987-1993.

14 M. Sametband, U. Shimanovich and A. Gedanken, *New J. Chem.,* 2012, 36, 36-39.

15 H. Q. Wang, L. C. Jia, P. Bogdanoff, S. Fiechter, H. Möhwald and D. Shchukin, *Envergy Eviron. Sci.,* 2013, **6**, 799-804.

16 H. Q. Wang, X. H. Yan, G. L. Li, C. Pilz-Allen, H. Möhwald and D. Shchukin, *Adv. Heathc. Mater.*, 2014, **3**, 825-831.

17 L. Zhang, V. Belova, H. Q. Wang, W. F. Dong and H. Möhwald, *Chem. Mater.,* 2014, **26**, 2244-2248.

18 X. Li, X. Wang, L. Zhang, S. Lee, H. Dai, *Science*, 2008, **319**, 1229-1232.

19 W. S. Hummers and R. E. Offeman, *J. Am. Chem. Soc.*, 1958, **80**, 1339-1339.

20 X. Sun, Z. Liu, K. Welsher, J. T. Robinson, A. Goodwin, S. Zaric and H. J. Dai, *Nano Res.*, 2008, **1**, 203-212.

21 M. Newville, *J. Synchrotron Rad.*, 2001, **8**, 96-100.

22 Y. B. Sun, J. X. Li and X. K. Wang, *Geochim. Cosmochim. Acta*, 2014, **140**, 621-643.

23 S. Stankovich, D. A. Dikin, G. H. B. Dommett, K. M. Kohlhaas, E. J. Zimney, E. A. Stach, R. D. Piner, S. T. Nguyen and R. S. Ruoff, *Nature*, 2006, **442**, 282-286.

24 D. W. Lee, T. K. Hong, D. Kang, J. Lee, M. Heo and J. Y. Kim, *J. Mater. Chem.*, 2011, **21**, 3438-3442.

25 A. C. Ferrari, J. C. Meyer, V. Scardaci, C. Casiraghi, M. Lazzeri, F. Mauri, S. Piscanec, D. Juang, K. S. Novoselov, S. Roth and A. K. Geim, *Phys. Rev. Lett.*, 2006, **97**, 187401-187404.

26 G. K. Ramesha and S. Sampath, *J. Phy. Chem. C*, 2009, **113**, 7985-7989.

27 T. Szabó, O. Berkesi, P. Forgó, K. Josepovits, Y. Sanakis, D. Petridis and I. Dékány, *Chem. Mater.*, 2006, **18**, 2740-2749.

28 D. Yang, A. Velamakannim, G. Bozoklu, S. Park, M. Stoller, R. D. Piner, S. Stankovich, I. Jung, D. A. Field, C. A. Ventrice Jr and R. S. Ruoff, *Carbon*, 2009, **47**, 145-152.

29 Y. Si and E. T. Samulski, *Nano Lett.,* 2008, **8**, 1679-1682.

30 A. Bagri, C. Mattevi, M. Acik, Y. J. Chabal, M. Chhowalla and V. B. Shenoy, *Nat. Chem.,* 2010, **2**, 581-587.

31 A.C. Ferrarl, J.C. Meyer, V. Scardacl, C. Caslraghl, M. Lazzerl, F. Maurl, S. Piscanec, D. Jiang, K.S. Novoselov, S. Roth, A. K. Geim, *Phys. Rev. Lett.*, 2006, **97**, 18704.

32 D. W. Lee, V. L. De Los Santos, J. W. Seo, L. leon Felix, D. A. Bustamante, J. M .Cole and C. H. W. Barnes, *J. Phys. Chem. B*, 2010, **114**, 5723-5728.

33 J. I. Paredes, S. Villar-Rodil, A. Martinez-Alonso and J. M. D. Tascon, *Langmuir*, 2008, **24**, 10560-10564.

34 T. Ramanathan, F. T. Fisher, R. S. Ruoff and L. C. Brinson, *Chem. Mater.,* 2005, **17**, 1290-1295.

35 Z. H. Sheng, L. Shao, J. J. Chen, W. J. Bao, F. B. Wang and X. H. Xia, *ACS Nano*, 2011, *5*, 4350-4358.

36 X. Fan, W. Peng, Y. Li, X. Li, S. Wang, G. Zhang and F. Zhang, *Adv. Mater.*, 2008, **20**, 4490-4493.

37 Y. B. Sun, C. L. Chen, D. D. Shao, J. X. Li, X. L. Tan, G. X. Zhao, S. B. Yang and X. K. Wang, *RSC Adv.,* 2012, **2**, 10359-10364.

38 Y. B. Sun, S. T. Yang, G. D. Sheng, Q. Wang, Z. Q. Guo and X. K. Wang, *Radiochim. Acta*, 2012, **100**, 779-784.

39 T. D. Waite, J. A. Davis, T. E. Payne, G. A. Waychunas and N. Xu, *Geochim. Cosmochim. Acta* 1994, **58**, 5465-5478.

40 Y. B. Sun, S. T. Yang, G. D. Sheng, Z. Q. Guo X. L. Tan, J. Z. Xu and X. K. Wang, *Sep. Purif. Technol.*, 2011, **83**, 196-203.

41 I. Chowdhury, M. C. Duch, N. D. Mansukhani, M. C. Hersam, D. Bouchard, *Environ. Sci. Technol.* **2013***, 47*, 6288-6296.

42 L. Wu, L. Liu, B. Gao, R. M. Carpena, M. Zhang, H. Chen, Z. H. Zhou, H. Wang, *Langmuir* **2013**, *29*, 15174-15181.

43 J. R. Bargar, R. Reitmeyer, J. J. Lenhart and J. A. Davis, *Geochim. Cosmochim. Acta*, 2000, **64**, 2737-2749.

Figure captions

Figure 1. HRTEM images (A and B) and AFM images (C and D) of GO0 and GO3.

Figure 2. Characterization of GO0, GO1, GO2 and GO3, A: Raman spectra; B: FT-IR spectra; C: UV/vis absorbance spectra; D: XPS spectra.

Figure 3. A: The effect of pH on U(VI) adsorption onto GO0, GO1, GO2 and GO3, T = 293 K, I = 0.01 mol/L $NaClO_4$; B: Adsorption isotherms of U(VI) on GO0, GO1, GO2 and GO3, pH 4.0, T = 293 K, I = 0.01 mol/L $NaClO_4$;

Figure 4. B: EXAFS spectra of U(VI)-reacted GO, pH 4.0, T = 293 K, I = 0.01 mol/L $NaClO_4$.

Table captions

Table 1. Fitting Results of U L_{III}-edge EXAFS spectra for reference samples and U(VI) –reacted GO0, GO1, GO2 and GO3, T = 293 K, I = 0.01 mol/L $NaClO_4$

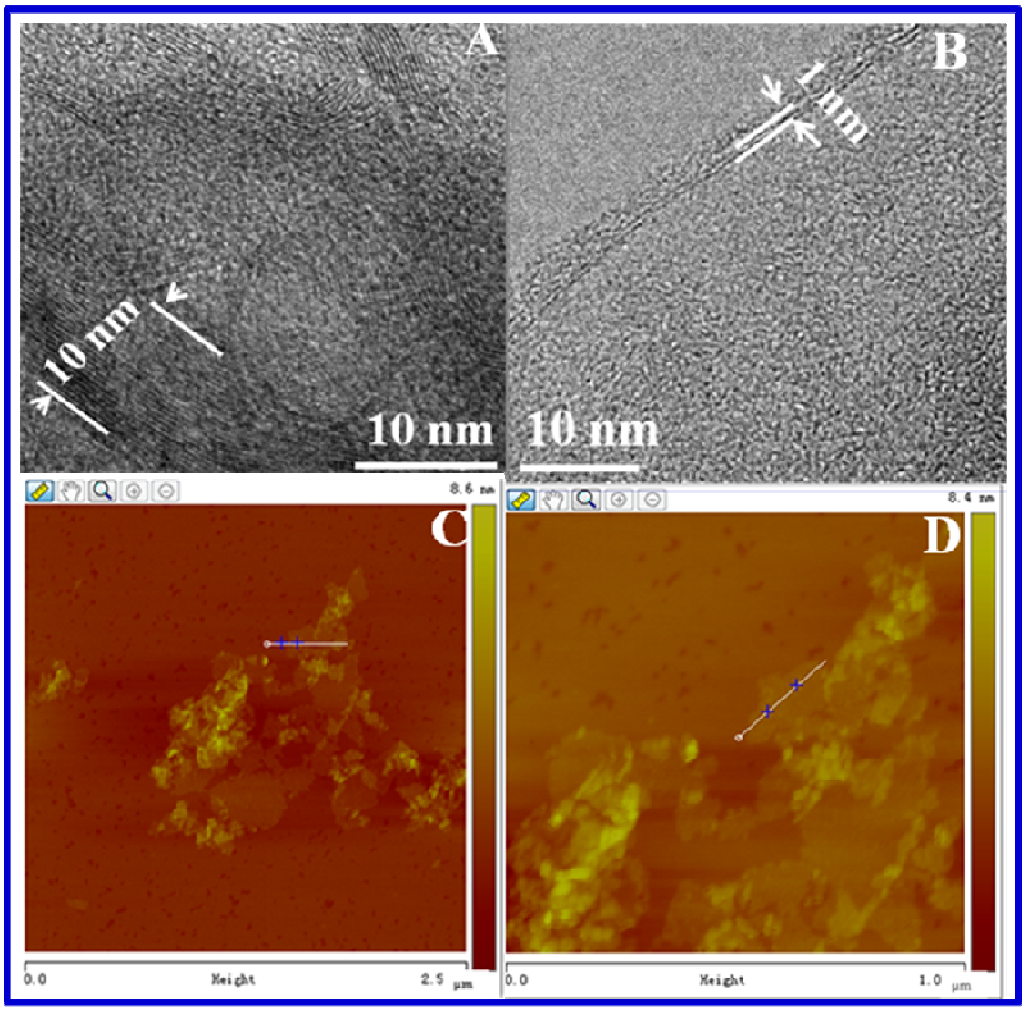

Figure 1

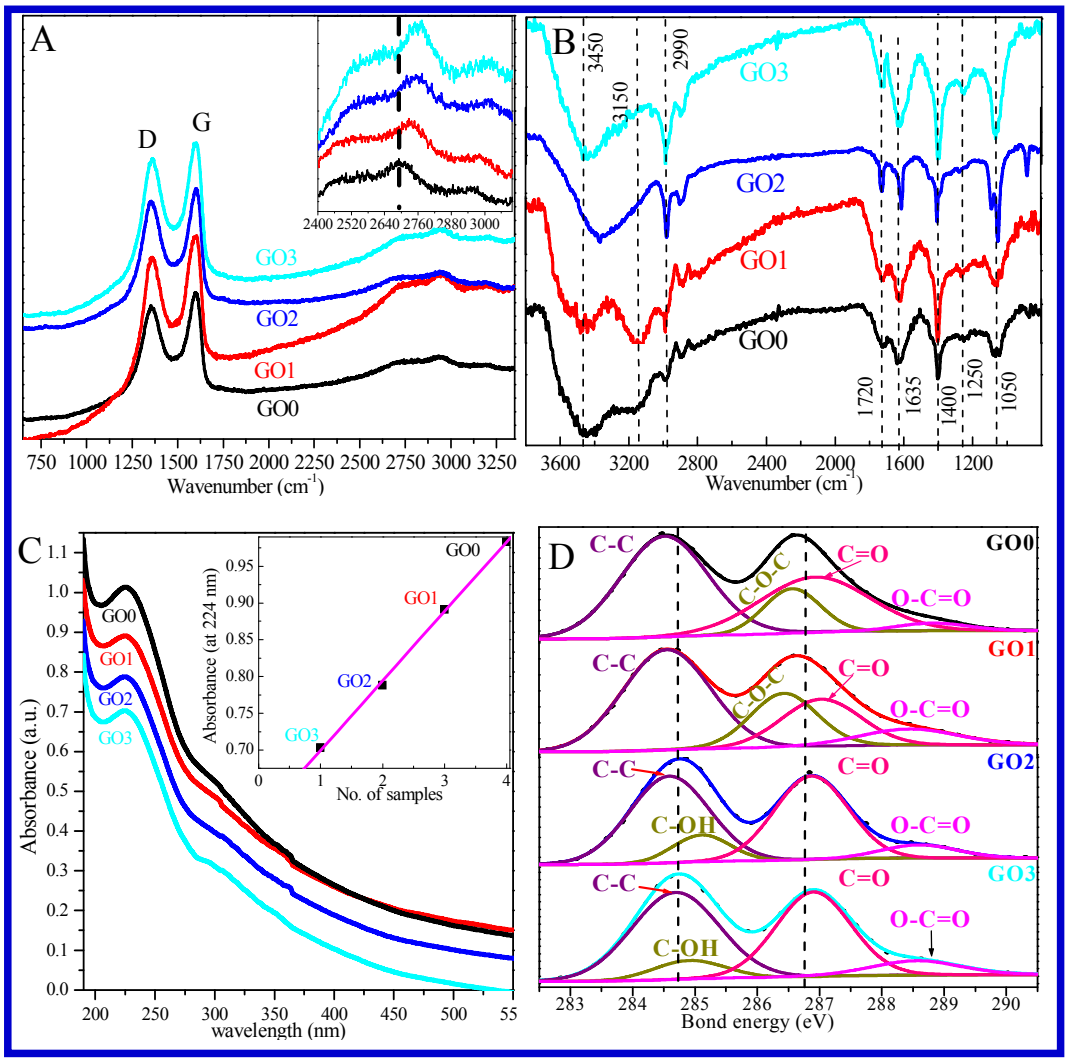

Figure 2

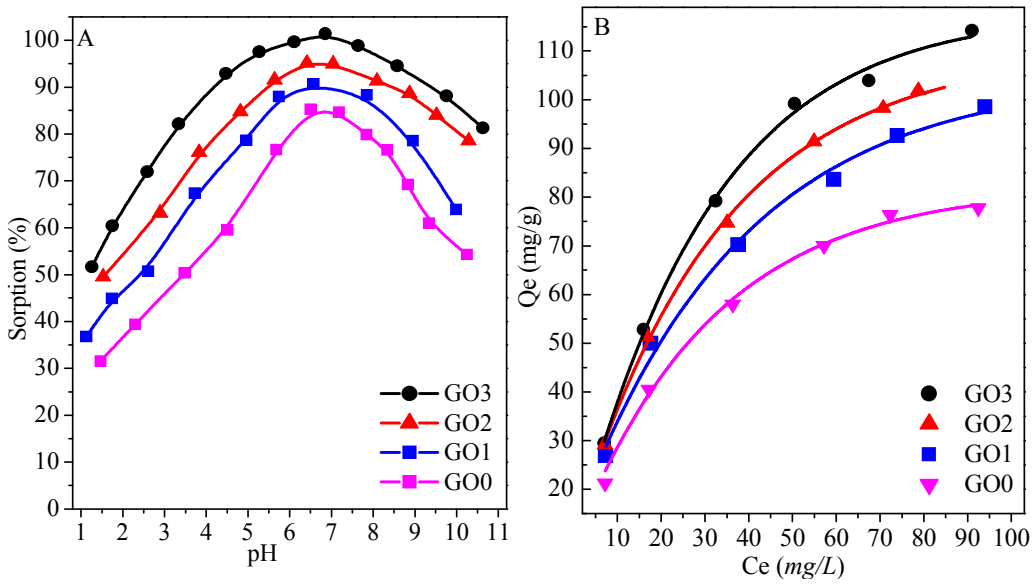

Figure 3

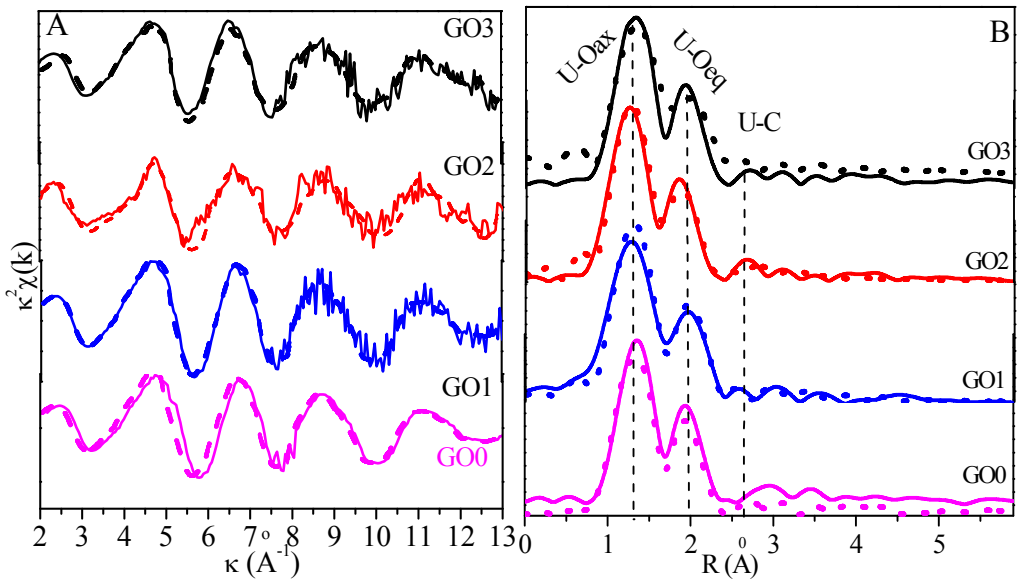

Figure 4

Table 1. Fitting Results of U L_{III}-edge EXAFS spectra for reference samples and U(VI) –reacted GO0, GO1, GO2 and GO3, T = 293 K, I = 0.01 mol/L $NaClO_4$

Samples	*Shell*	*R(Å)* [a]	*CN* [b]	σ^2 *(Å²)* [c]
UO_3	U-O_{ax}	1.740(8)	1.8(7)	0.00466
	U-O_{eq}	2.253(9)	5.5(5)	0.0057
	U-U	3.853(2)	0.2(3)	0.0167
U(VI)(aq)	U-O_{ax}	1.826(0)	1. 9(5)	0.0076
	U-O_{eq}	2.577(1)	6.2(7)	0.0051
	U-U	4.096(9)	1.9(5)	0.0053
GO0	U-O_{ax}	1.8049(6)	2.0(0)	0.00309
	U-O_{eq}	2.4277(0)	4.9(9)	0.00834
GO1	U-O_{ax}	1.7874(6)	2.0(0)	0.00381
	U-O_{eq}	2.4099(0)	4.5(9)	0.00592
	U-C	3.2308(1)	1.1(3)	0.01050
GO2	U-O_{ax}	1.8088(0)	2.0(0)	0.00545
	U-O_{eq}	2.4446(0)	4.2(3)	0.00627
	U-C	3.3100(7)	1.7(8)	0.00180
GO3	U-O_{ax}	1.8088(0)	2.0(0)	0.00545
	U-O_{eq}	2.4304(0)	5.0(2)	0.00139
	U-C	3.3115(6)	1.7(7)	0.00257

[a] R is the bond distance; [b] CN is coordination numbers of neighbors; [c] σ^2 is the Debye-Waller factor.

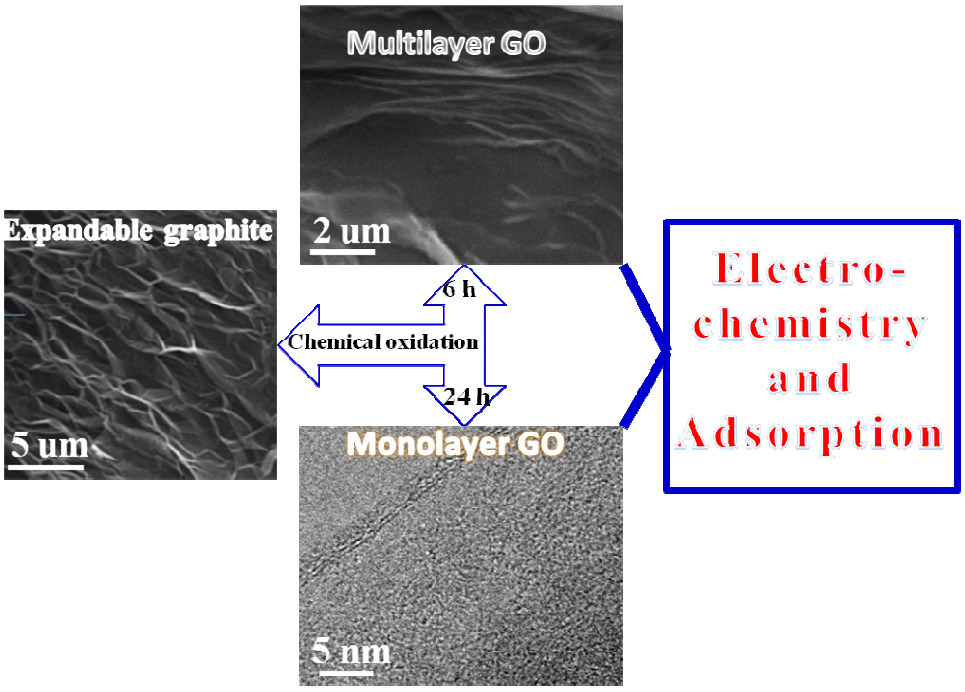

Schematic 1. A schematic diagram of the synthesis protocol.